Influence of transition group elements on the stability of the delta- and eta-phase in nickelbase alloys

Influence of transition group elements on the stability of the δ- and η-phase in nickelbase alloys

Martin Bäker[1], Joachim Rösler[1], Tatiana Hentrich[2], Graeme Ackland[3]

October 5, 2017

[1] Institut für Werkstoffe, Langer Kamp 8, 38106 Braunschweig, Germany
[2] VDM Metals International GmbH, Plettenberger Strasse 2, 58791 Werdohl, Germany
[3] School of Physics & Astronomy, The University of Edinburgh, Peter Guthrie Tait Road, Edinburgh EH9 3FD, Scotland

Abstract

To improve the high-temperature capability of 718-type wrought nickel-base superalloys, the γ'-phase (Ni_3Al) can be stabilized. However, this also reduces the size of the forging window because forging has to be done above the γ'- and below the solvus temperature of the phase that is used to enable fine-grain forging, i. e. the δ-phase of Ni_3Nb type or the η-phase of Ni_3Ti-type. Understanding the influence of alloying elements on the formation of these phases is therefore important. In this paper, density functional theory calculations at 0K are performed to determine the stabilizing effect of aluminium and of the transition group elements on the stability of the δ-phase and η-phase. Most of the transition group elements of 5th and 6th period stabilize the δ-phase, whereas the stabilizing effect on the η-phase is weaker. According to the calculations, Mo, Tc, W, Re, and Os may be expected to stabilize the δ-phase but not the η-phase, whereas Al and Zn strongly stabilize the η-phase. V, Zr, Ru, Rh, Pd, Ag, Cd, Hf, Ta, Ir, Pt, Au, and Hg stabilize both phases. For some elements (Cr, Mn, Fe, Co), magnetic effects in the δ and especially in the η-phase are shown to be significant at the concentrations studied here.

Keywords nickel alloys, nickel-base superalloys, phase stability, density functional theory

1 Introduction

Alloys 718 and 706 belong to a special class of materials among the Ni-based superalloys. These so-called 718-type materials excel due to their outstanding manufacturability and high strength up to service temperatures of about 650 °C. Therefore, they are materials of choice for highly loaded turbine discs in aircraft engines amongst other components [1, 2]. Alloy 718 alone accounts for about two-thirds of the weight of superalloys in aircraft engines [3].

718-type superalloys are strengthened by the γ' and γ''-phases. These phases have to be stable at service temperature, but are dissolved during forging to ensure sufficient malleability of the alloy. Additional phases that are stable at higher temperatures are used to hinder grain growth during the forging process, thus ensuring a fine grained microstructure [4]. These phases are either the δ-phase (Ni_3Nb, Strukturbericht designation DO_a) or the η-phase (Ni_3Ti, Strukturbericht designation DO_{24}). Consequently, 718-type superalloys are designed such that the solvus temperature of the strengthening phases is above service temperature but below forging temperature, while the δ/η-phase is stable up to the forging temperature. In other words, the solvus temperature of the δ/η-phase must exceed that of the strengthening phases.

Due to ever increasing temperatures in gas turbines, there is demand for 718-type alloys allowing for higher application temperatures. This requires improved stability of the strengthening phases, which can be readily achieved increasing the Al-content of the alloy as it is done in the alloy 718Plus [5] and VDM Alloy 780 [6]. However, if the γ' solvus temperature is increased, the forging temperature has to be increased as well. This, in turn, requires raising the thermal stability of the δ/η-phase. In designing new wrought nickel-based superalloys with increased temperature stability, it is thus necessary to understand the influence of alloying elements on the stability of the δ- and η-phase.

In this paper, DFT simulations at 0K are used to determine the solution energy of aluminium and transition group elements in the δ-phase and η-phase to understand which elements can stabilize these phases. (Detailed

calculations for the influence of the most important alloying elements on the γ'-phase can be found in [7].) These elements have been selected because the metallic alloying elements in nickelbase superalloys are either transition group elements or aluminium. The stabilizing effect on both phases is compared to aid the design of future alloys.

2 Theory and Methods

2.1 Calculation method

Density functional theory calculations at 0K were performed using VASP [8, 9, 10]. A plane wave bases set with projected augmented wave (PAW) pseudopotentials [11, 12] was used in the simulations together with Perdew-Burke-Ernzerhof [13] exchange correlation functionals. Where available, pseudopotentials including full simulation of s- or p-electrons (i. e. the maximum valency available) have been used. The energy cutoff (ENCUT) was chosen as 520 eV in all simulations, a value that is 1.3 times the largest cutoff value provided in the PBE files of all elements simulated as recommended in the VASP manual to ensure that absolute energies are calculated to high precision. Calculations were usually spin-polarized, with some exceptions for calculations within the δ/η-phase where both polarized and non-polarized calculations were performed for some elements as explained below.

The spacing of the k-points in the reciprocal lattice was chosen as 0.1 Å^{-1}; resulting in k-point grids of 9^3 for the γ-cell, $8 \cdot 13 \cdot 7$ for the δ-cell and $13 \cdot 8 \cdot 8$ for the η-cell. (Each of the cells contained 32 atoms, see below.) For the γ-cell consisting of pure Ni, a smaller spacing of 0.07 Å^{-1} did result in an energy difference of less than 0.01 meV per atom. For the η-cell, increasing the k-point grid to $18 \cdot 11 \cdot 11$ changed the energy by less than 0.02 meV per atom. All calculations except for the pure element energies were performed for 32-atom supercell to avoid effects from different atom numbers.

The precision of the calculation was set to "accurate" to avoid wrap around errors; the real space operators were calculate to a precision of 10^{-4} (`ROPT=1e-4`). Intermediate runs to determine the optimum lattice parameters were performed with an electronic precision of 10^{-3} meV (`EDIFF` =1.E-6), the final runs with 10^{-4} meV. The ionic loop during relaxation was stopped when the energy change was below 10^{-2} meV (`EDIFFG` =1.E-5).

To check the influence of the size of the chosen 32-atom supercell and

possible self-interaction of the atoms, calculations with a fully relaxed larger 256-atom γ-supercell were done for two elements, V and Nb. The substitution energies differed by 11.6 meV for V and 1.3 meV for Nb. Calculations with a 32-atom cell therefore do not correspond to the strict dilute limit.

For each of the considered atomic configurations, the lattice constant and lattice shape as well as the ionic positions were relaxed. To do so, we employed the following two-step procedure as recommended in the VASP manual [14]: In a first step, calculations at fixed lattice volume were performed for five different volumes by simply changing the scale factor in the definition of the initial grid. Each of these calculations was at constant volume performed with relaxation of the ions (`ISIF` $= 2$) for the γ-phase and with relaxation of the ions and the cell shape (`ISIF` $= 4$) for the δ and η-phase. These calculations were performed with Gaussian smearing and a smearing parameter of 0.07 eV. (These values were taken from [7].)

A Birch-Murnaghan state equation [15] was used to fit the energies and determine the optimum scale factor. A final calculation using this scale factor was performed, using the fixed final ionic positions of the run with the closest scale factor. In this final calculation, a tetrahedral mesh with Blöchl correction was used.

This method results in lower energies compared to those calculated by simply relaxing the cell shape, size and ions in one step (`ISIF` $= 3$). For example, for a 32-atom η-phase supercell, the energy calculated using `ISIF` $=$ 3 and then performing a final calculation with fixed lattice and ions is 21 meV larger than the final energy obtained in the way described here; for a $Ni_{31}Nb$-cell, the final energy is 39 meV larger using the direct relaxation.

2.2 Pure element calculations

The main purpose of this study is the comparison between the solution energies in the three phases considered here (γ, δ, η). In this comparison, the energy to transport the element under consideration from one phase to another is calculated (see eqs. (4) and (5)) and pure element energies are not needed. Nevertheless, pure element energies allow to report substitution energies for single phases and are therefore helpful as reference quantities. For Nb and Ti, calculating the energy of the pure element also serves as a check on phase stability (see section 3.3 and 3.4).

Most of the elements considered have a bcc, fcc or hcp lattice structure. Exceptions are mercury with a rhombohedral lattice structure and

manganese with a complicated, 29-atom unit cell. For fcc and bcc elements, a conventional unit cell was used; for hcp elements, a 2-atom cell was employed. The initial configurations of all unit cells were taken from the open quantum molecular database [16] with the exception of the 29-atom Mn cell which was taken from [17]. For Co, both an fcc and an hcp structure were calculated due to the small difference in their energy.

For all elements considered, the element lattice was relaxed as described in the previous section; allowing for ionic relaxation in the cubic elements and for ionic and cell shape relaxation for the hcp and the rhombohedral Hg lattice. All cells were initialized with a ferromagnetic state. The only exception was Cr where a 2-atom anti-ferromagnetic bcc configuration was used.

2.3 Substitution in the γ-phase

A 32-atom (2^3 conventional fcc) cell was used for the γ-phase; replacing one atom with the alloying atom under consideration. The γ-phase is ferromagnetic; alloying atoms may possess moment aligned with (ferromagnetic) or opposite to (ferrimagnetic) the nickel atoms.. To check for magnetic effects in $Ni_{31}X$, calculations with the initial magnetic moment of the alloying element being aligned or opposite to that of the nickel atoms (setting the moment of this atom to $\pm 1\mu_B$, that of all Ni atoms to $1\mu_B$) were performed, using a fixed lattice constant and slightly loosened convergence criteria to save CPU time. For most elements, both simulations converged to the same state. Exceptions were Mn and Fe, where the final configuration with an opposite moment had a considerably higher energy than the ferromagnetic configuration, Cr, where the final configuration with opposite moment is energetically favourable, and Co, where the computation with opposite moment did not converge.

To calculate the final energies of the $Ni_{31}X$ supercells, the lattice constant was relaxed as described above. Based on the results for the ferro- and ferrimagnetic initialization as described in the previous paragraph, all configurations except for $Ni_{31}Cr$ were initialized with a purely ferromagnetic state. It should be noted that the ferrimagnetic state of the Cr atom might change in a larger supercell (corresponding to the dilute limit); but in the alloys under consideration in this study, the Chromium content is usually large as will be discussed further below (section 4).

The substitution energy of each element was calculated as

$$E_{\mathrm{X},\gamma} = E(\mathrm{Ni_{31}X}) - (31E(\mathrm{Ni}) + E(\mathrm{X})) \tag{1}$$

where $E(\ )$ denotes the calculated energy of the structure or element.

2.4 Substitution in the δ-phase

Calculations for the pure δ-phase (Ni_3Nb) were done with a 32-atom supercell configuration taken from the open quantum molecular database OQMD [16]. The structure was relaxed as explained in section 2.1. Spin-polarized calculations were performed to check that the calculated end-state was unmagnetic.

To calculate alloying effects for the alloying elements under consideration, one atom in the supercell was replaced. There are three distinct possibilities to substitute one atom in the δ-phase, as calculated with SOD [18]: two for substituting Ni, one for Nb. These configurations are shown in Fig. 1. For each calculation, the lattice relaxation algorithm from section 2.1 was used.

All calculations were spin-polarized (starting from a ferro-magnetic cell) to check whether magnetic effects might play a role. For those elements where atoms in the final configuration possessed a non-negligible magnetic moment, non-polarized calculations were also performed to see the strength of the effect.

The solution energy for an element in the δ-phase ist calculated using the δ-phase, the pure γ-phase and the pure element as a reference state. The energy depends on where the solution element is situated in the lattice. If the atom sits on a Nb position, dissolving it in the δ-phase requires to transfer three Ni atoms from the γ to the δ-phase because the Nb atom has the lowest energy in the δ-phase and will thus not shift to another phase. To replace Ni, a single Ni atom is shifted from the δ to the γ-phase. The solution energies are therefore calculated as

$$E_{\mathrm{X},\delta,\mathrm{Nb}} = E(\mathrm{Ni_{24}Nb_7X}) - (7E(\mathrm{Ni_3Nb}) + 3E(\mathrm{Ni}) + E(\mathrm{X})) \tag{2}$$

$$E_{\mathrm{X},\delta,\mathrm{Ni}} = E(\mathrm{Ni_{23}Nb_8X}) + E(\mathrm{Ni}) - (E(\mathrm{Ni_{24}Nb_8}) + E(\mathrm{X}))\ . \tag{3}$$

To see whether an element dissolves in the γ- or in the δ-phase, the

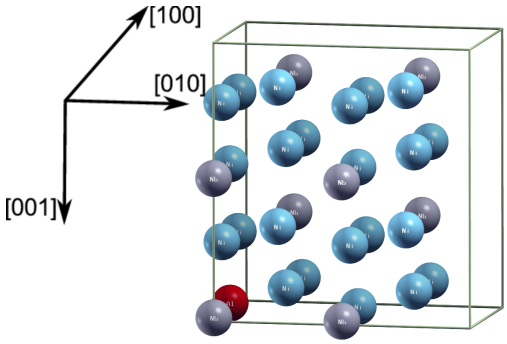

(a) Substituting for Ni (Ni1) – $(Ni_3Nb)_7\,Ni_2NbX$

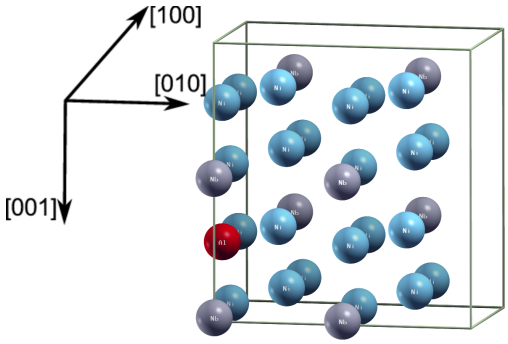

(b) Substituting for Ni (Ni2) – $(Ni_3Nb)_7\,Ni_2NbX$

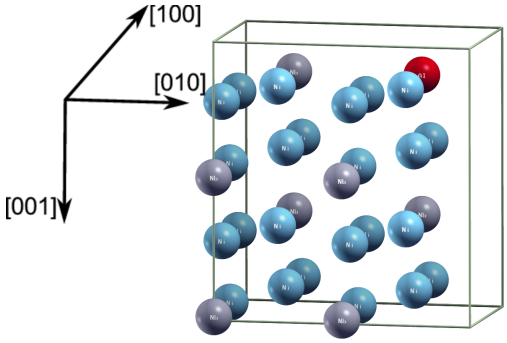

(c) Substituting for Nb – $(Ni_3Nb)_7\,Ni3X$

Figure 1: Substitution of one alloying atom for Ni or Nb in the δ phase (Ni atoms in blue, Nb atoms in grey, alloying atom in red).

difference in the solution energies is calculated:

$$\begin{aligned} E_{\mathrm{X,Diff,\ }\delta\mathrm{,Nb}} &= E_{\mathrm{X},\delta,\mathrm{Nb}} - E_{\mathrm{X},\gamma} \\ &= E(\mathrm{Ni_{24}Nb_7X}) + 28E(\mathrm{Ni}) - 7E(\mathrm{Ni_3Nb}) - E(\mathrm{Ni_{31}X}) \qquad (4) \\ E_{\mathrm{X,Diff,\ }\delta\mathrm{,Ni}} &= E_{\mathrm{X},\delta,\mathrm{Ni}} - E_{\mathrm{X},\gamma} \\ &= E(\mathrm{Ni_{23}Nb_8X}) + 32E(\mathrm{Ni}) - E(\mathrm{Ni_{24}Nb_8}) - E(\mathrm{Ni_{31}X})\,. \qquad (5) \end{aligned}$$

2.5 Substitution in the η-phase

The strategy for the calculations of the η-phase was the same as for the δ-phase. The initial configuration was again taken from the OQMD and relaxed. Afterwards, substitutions of the alloying elements were calculated. Fig. 2 shows the possible replacements in the 32-atom cell of the η-phase (two each for the Ti and the Ni substitution).

The η-phase itself was found to be unmagnetic, but there are magnetic effects for several alloying elements. For these, non-spin-polarized calculations were performed as well.

Solution energies were calculated in the same way as for the δ-phase, see eqs. (2)–(5), replacing Ti for Nb.

3 Results

3.1 Pure elements

Table 1 shows the calculated energy per atom for each of the considered elements. For those elements were calculations with the same pseudopotential were avaliable in the OQMD [16], agreement between our calculations and the OQMD results was usually within less than 3 meV. Exceptions were elements for which our lattice relaxation method yields considerably different lattice constants (Ag, Cd, Au, Hg). For these elements, deviations in the energies of up to 17 meV occured, and lattice parameters differed by 1% or more. Since the OQMD results were obtained using a direct relaxation of the cell size in a single calculation, this difference can be explained by the different calculation method to obtain the relaxed ground state (see section 2.1).

For Pd, initializing with a ferromagnetic state results in an end state with a small magnetic moment on each Pd atom. The energy of this structure is

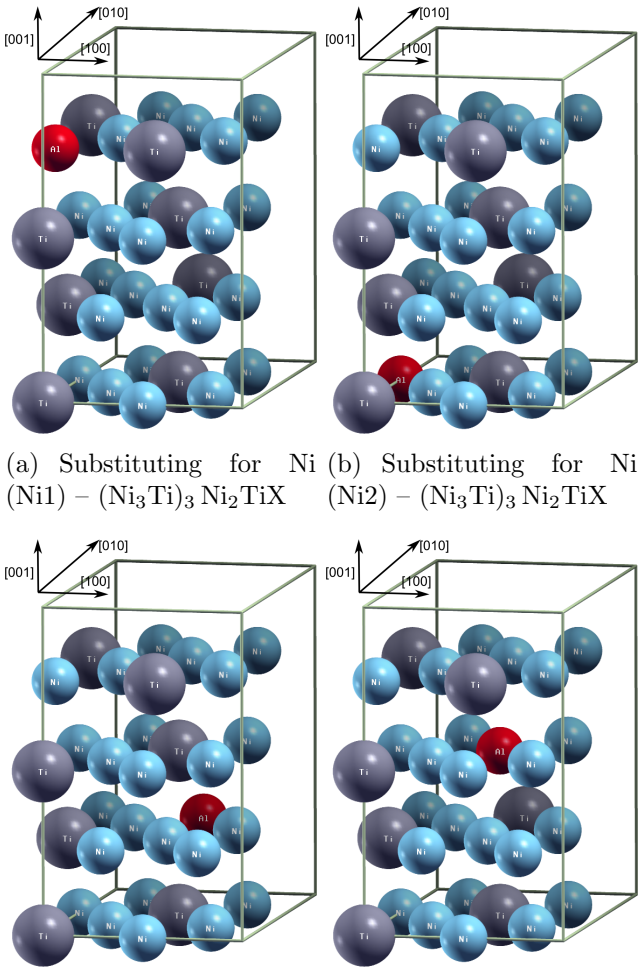

(a) Substituting for Ni (Ni1) – $(Ni_3Ti)_3\,Ni_2TiX$

(b) Substituting for Ni (Ni2) – $(Ni_3Ti)_3\,Ni_2TiX$

(c) Substituting for Ti (Ti1) – $(Ni_3Ti)_3\,Ni_3X$

(d) Substituting for Ti (Ti2) – $(Ni_3Ti)_3\,Ni_3X$

Figure 2: Substitution of one alloying atom for Ni or Ti in the η phase (Ni atoms in blue, Ti atoms in grey, alloying atom in red).

Table 1: Calculated energy per atom of the pure alloying elements.

Element	**structure**	**Energy** / eV/atom
Al	fcc	-3.7461
Ti	hcp	-7.9461
V	bcc	-9.1193
Cr	bcc	-9.6462
Mn	cub	-9.1528
Fe	bcc	-8.4568
Co	hcp	-7.1084
	fcc	-7.0906
Ni	fcc	-5.7792
Cu	fcc	-4.0985
Zn	hcp	-1.2660
Zr	hcp	-8.5471
Nb	bcc	-10.2252
Mo	bcc	-10.8490
Tc	hcp	-10.3622
Ru	hcp	-10.3622
Rh	fcc	-7.3445
Pd	fcc	-5.3860
Ag	fcc	-2.8283
Cd	hcp	-0.8865
Hf	hcp	-9.9560
Ta	bcc	-11.8531
W	bcc	-12.9613
Re	hcp	-12.4461
Os	hcp	-11.2266
Ir	fcc	-8.8573
Pt	fcc	-6.0571
Au	fcc	-3.2723
Hg	rhl	-0.2956

1.7 meV lower than the energy of a Pd atom in a non-spin-polarized calculation. In the calculations of the substitution energies, the lower energy value was used. For Co, both an fcc and an hcp structure were calculated because the energy of both phases is known to be very similar. In our calculation, the energy of the hcp is slightly smaller than that of the fcc structure.

Note that the results of the pure element energies are relevant for the substitution energies, but not for a comparison of these energies (the question whether an element would transfer to δ/η from γ).

3.2 γ-phase

The energy of a nickel atom of the pure γ-phase is reported in Table. 1; the calculated lattice constant was 3.523 Å. Substituting one nickel atom by an alloying element in the 32-atom supercell corresponds to a concentration of 3.125%. The calculated change in the lattice constant can be used to predict the influence of the alloying elements on the lattice constant. In Fig. 3, the change in the lattice constant is shown for all elements and compared with data from [19] where data is available. With the exception of Os, the agreement between the calculation and the experimental results is satisfactory.

The calculated substitution energies for all elements in the γ-phase are shown in Fig. 4. Positive values in the diagram do not imply that the considered element cannot be used in alloying because many of the transition element have a finite solubility in nickel at typical processing temperatures of the order of 1000 °C.

3.3 δ-phase

To check whether the δ-phase is stable, we calculate the energy of $Ni_3 + Nb$ in three different states (dissolved in γ, as a δ cell or as isolated nickel and niobium phases):

$$\begin{aligned} E_{\text{solution}} &= E(\text{Ni}_{31}\text{Nb}) - 28E(\text{Ni}) && = -28.2496\,\text{eV} \\ E_{\delta} &= \frac{1}{8}E(\text{Ni}_{24}\text{Nb}_8) && = -28.8134\,\text{eV} \\ E_{\text{separated}} &= E(\text{Nb}) + 3E(\text{Ni}) && = -27.4329\,\text{eV}\,. \end{aligned}$$

Formation of the δ-phase from the γ-phase is thus energetically favorable by 564 meV per Niobium atom. Note that other phases (like NiNb) were not

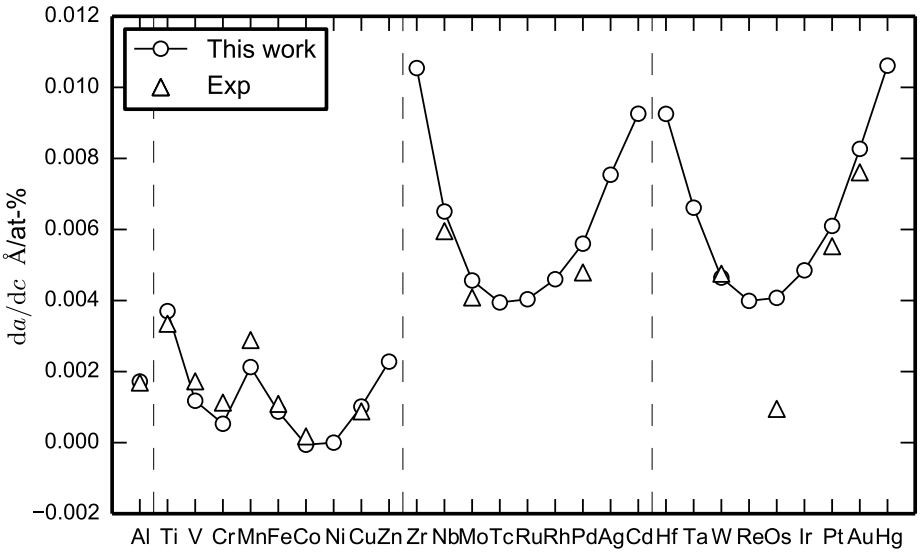

Figure 3: Predicted change in the lattice constant (in $\mathring{A}$) per at.-% of an alloying element (da/dc) compared to the experimental results reported in [19].

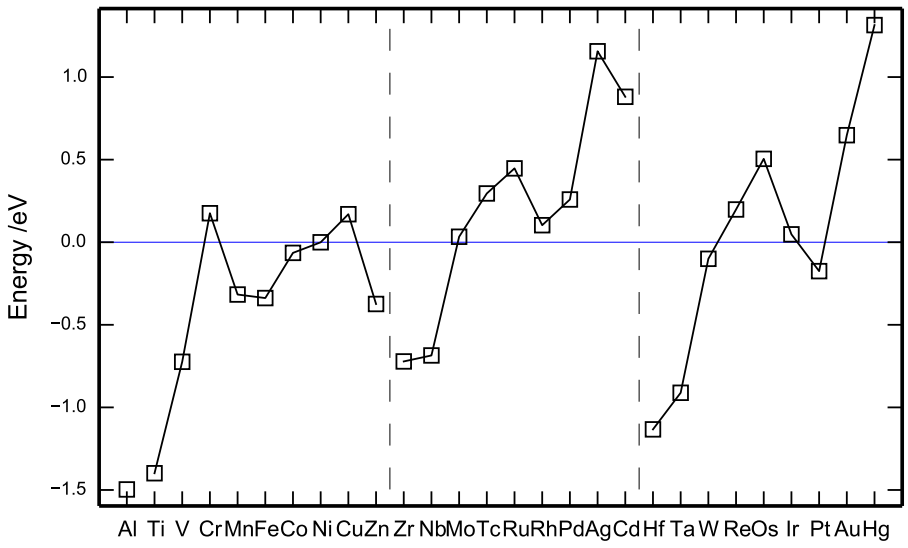

Figure 4: Substitution energies for the considered alloying elements in the γ-phase, calculated from eq. (1)

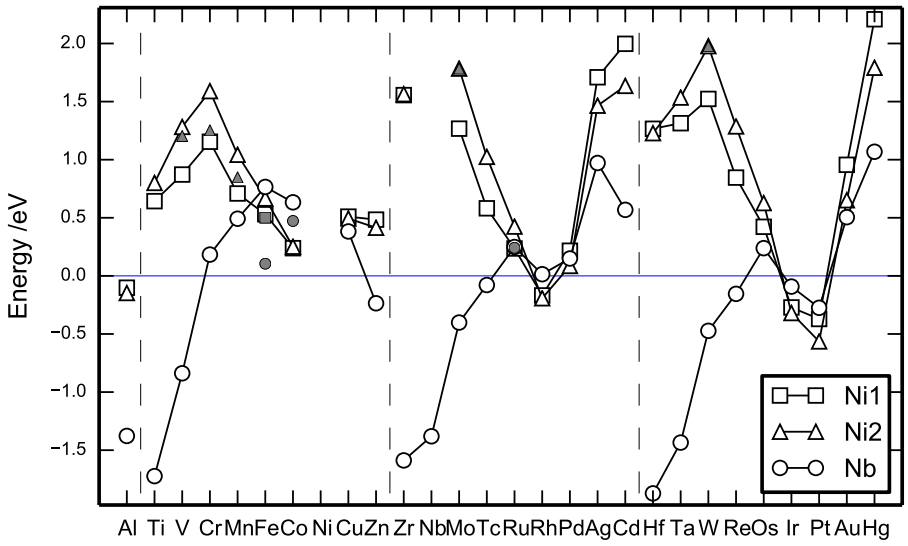

Figure 5: Substitution energies for an element in the δ-phase, calculated from eqs. (2) and (3). Grey symbols denote lowest-energy states with a magnetic moment in the δ-phase. For Nb, the energy difference between the δ-phase and the separate pure Ni and Nb phases has been plotted.

considered here because they do not occur in the alloys under consideration, so the stability is only shown with respect to pure Nb and solution in the γ-phase. As expected, the δ-phase was unmagnetic.

The calculated lattice constants of the δ-phase were 5.123 Å, 4.258 Å, and 4.562 Å. These values agree to within 1% with measured values from the literature [20] and with other DFT calculations [21].

Fig. 5 shows the substitution energies of the considered elements (using the pure δ-phase, pure nickel and the pure element as a reference state), calculated from eqs. (2) and (3). For some elements a non-zero magnetic moment was found as lowest energy state in the 32-atom δ-supercell. For these elements, an additional non-spin-polarized calculation (including lattice relaxation) was performed. The energy of the magnetic state is shown in the Figure (grey symbols). The substitution of a nickel atom in the δ-phase becomes energetically more favourable with increasing number of d-electrons as should be expected. The energy rises again if the number of d-electrons

Table 2: Predicted substitution behaviour in the δ-phase of different elements from [22] compared to the DFT calculations from figure 6. For iron, the calculated lowest energy state depends on whether a ferromagnetic (replace Nb) or a non-ferromagnetic state (replace Ni) in the δ-phase is considered.

	Al	Ti	V	Cr	Mn	Fe	Co	Cu
[22]	Nb	Nb	Nb	Nb	Nb	Ni/Nb	Ni	Nb
This work	Nb	Nb	Nb	Nb	Nb	Ni/Nb	Ni	Nb

	Zr	Mo	Pd	Hf	Ta	W	Re	Os	Ir	Pt	Au
[22]	Nb	Nb	Ni	Nb	Nb	Nb	Ni	Ni	Ni	Ni	Ni
This work	Nb	Nb	Ni	Nb	Nb	Nb	Nb	Nb	Ni	Ni	Nb

is larger than that of nickel. Substituting Nb is favorable for elements with a low number of d-electrons.

In [22], a thermodynamic model was used to determine the solution behaviour of several elements in different Ni_3M phases. The model was used to predict whether solution elements are situated on Ni or Nb sites in the δ-phase. Table 2 shows a comparison between the predictions of [22] and the current work for the site preference of the elements. For most of the elements, predictions do agree, but there is a discrepancy for Re, Os, and Au. For Os and Au, the calculated energy differences are small, but the difference is large for Re.

Fig. 6 shows the energy of transferring an alloying element from the γ to the δ-phase in a Ni or Nb position. (Data points in this figure can be obtained as difference between the results from Fig. 4 and Fig. 5.) Overall, substituting nickel in the δ-phase is not favoured for any of the elements in the Ti-period. In the higher periods, substituting nickel is favourable for Ru, Rh, Pd, Os, Ir, and Pt. From Fig. 5, it might seem that some of these elements (Ru, Pd, and Os) would not dissolve in the γ or the δ-phase, but at finite temperatures, these elements have a finite solubility in the γ matrix. During formation of the δ-phase, these elements may then be expected to dissolve in the more favourable phase.

On the other hand, elements with a low number of d-electrons, especially those in higher periods, can replace a niobium atom. (Note that the energy gain of the δ-phase formation has been entered into the figure in the Nb position.) It has to be noted, however, that these elements may form other phases like Ni_3Ti.

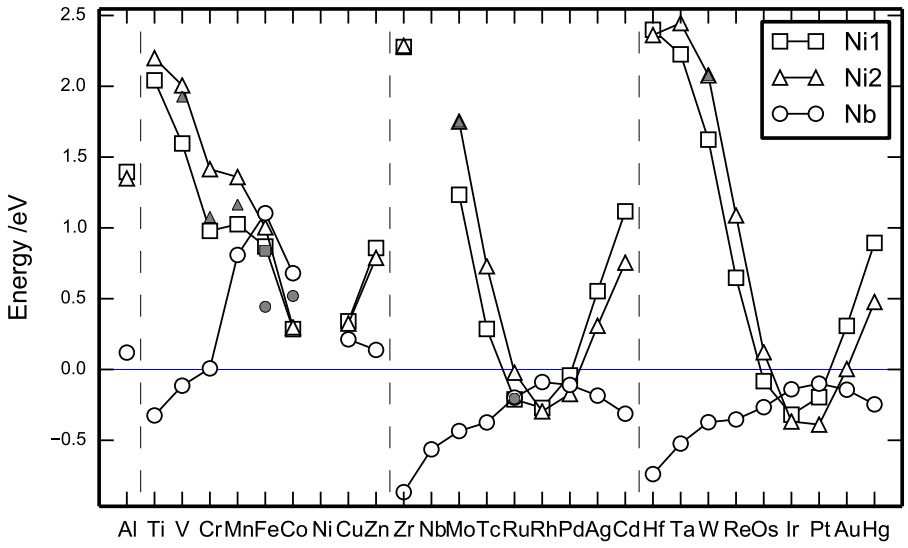

Figure 6: Energy difference between an alloying element in the δ and in the γ-phase, calculated from eqs. (4) and (5). For Nb, the energy difference between the δ-phase and a dissolved Nb in the γ-phase is shown. Grey symbols denote lowest-energy states with a magnetic moment in the δ-phase.

For most of those elements where a non-zero magnetic moment was found as lowest energy state in the 32-atom δ-supercell, the substitution energy for a transfer from γ to δ remains positive so that this effect will not affect the solution behaviour. The only exception is Ru where the magnetic state lowers the energy by only 6.6 meV.

3.4 η-phase

We calculated the stability of the η-phase in the same way as for the δ-phase; again disregarding other phases like NiTi:

$$\begin{aligned} E_{\text{solution}} &= E(\text{Ni}_{31}\text{Ti}) - 28E(\text{Ni}) && = -26.6836\,\text{eV} \\ E_{\delta} &= \frac{1}{8}E(\text{Ni}_{24}\text{Ti}_{8}) && = -27.2239\,\text{eV} \\ E_{\text{separated}} &= E(\text{Ti}) + 3E(\text{Ni}) && = -25.2850\,\text{eV}\,. \end{aligned}$$

Formation of the η-phase from the γ-phase is thus energetically favorable by 540 meV per titanium atom.

The calculated lattice constants for the conventional 32-atom unit cell were $a = 5.116\,\text{Å}$ in the basal plane and $c = 8.346\,\text{Å}$, close to the values of 5.115 Å and 8.302 Å given in [23].

Fig. 7 shows the substitution energies of the considered elements (using the pure δ-phase, pure nickel and the pure element as a reference state), calculated in the same way as for the δ-phase. A ferromagnetic state was found as ground state for several elements (marked by grey symbols in Fig. 7). The effect is especially strong for Cr, Mn, Fe, and Co in a Ti position of the η-phase, where the energy is lowered considerably.

Fig. 8 shows the energy of transferring an alloying element from the γ to the η-phase in a Ni or Ti position. The overall shape of the curves is similar to those for the δ-phase. Substituting a nickel atom in the η-phase is most favourable for atoms with a similar number of d-electrons, but only Ru, Rh, Pd, Ir, and Pt can be expected to actually stabilize the η-phase in this way. Substituting Ti is favourable for Al, Zn, Zr, Nb, Cd, Hf, Ta and Hg. A slight stabilization effect might be expected for V, Mo, Ag, and W, but the energies are small compared to typical thermal energies at the forging temperature.

Ferromagnetic effects in the η-phase are especially strong for Cr, Mn, Fe, and Co in a Ti position of the η-phase. For Cr and Mn, the energy to transfer an atom to the η-phase energy becomes slightly negative (of the order

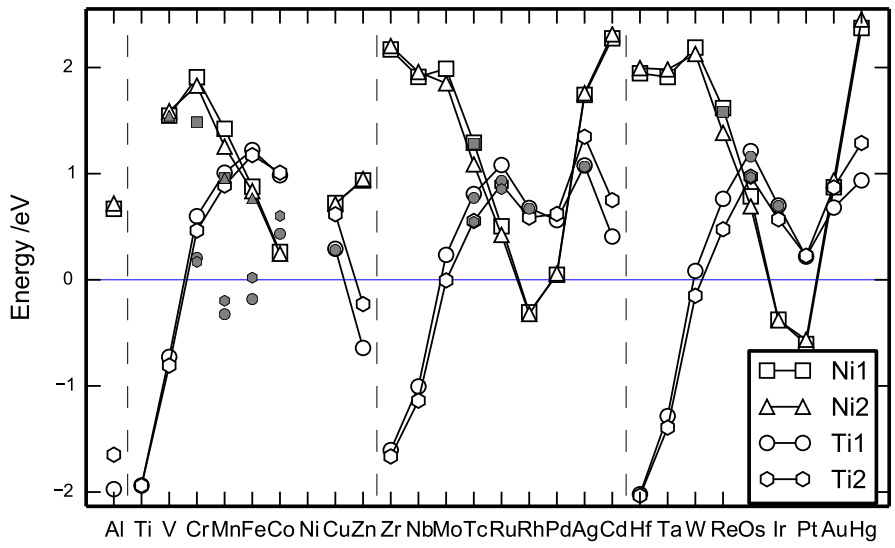

Figure 7: Substitution energies for an element in the η-phase, calculated from eqs. (2) and (3). Grey symbols denote lowest-energy states with a magnetic moment in the η-phase. For Ti, the energy difference between the η-phase and the separate pure Ni and Ti phases has been plotted.

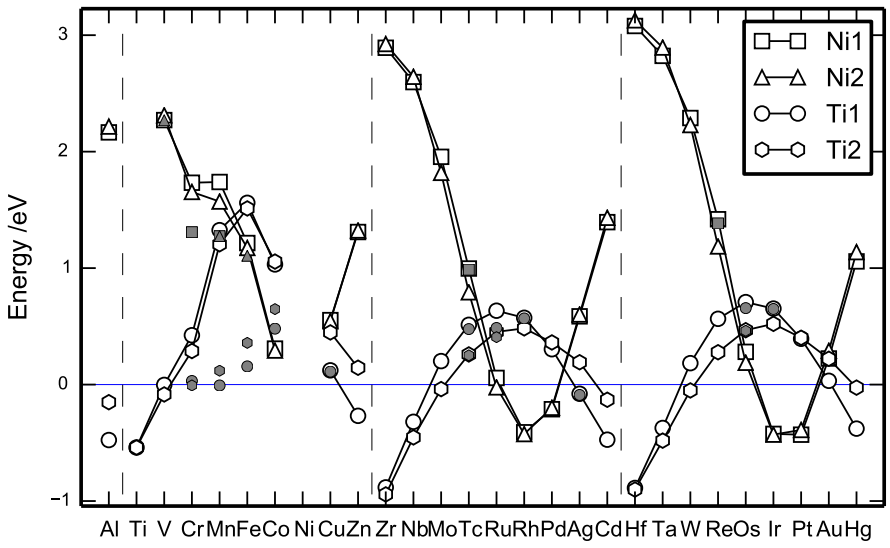

Figure 8: Energy difference between an alloying element in the η and in the γ-phase, calculated from eqs. (4) and (5); replacing Ti for Nb. For Ti, the energy difference between the η-phase and a dissolved Ti in the γ-phase is shown. Grey symbols denote lowest-energy states with a magnetic moment in the η-phase.

of 7 meV). These magnetic effects might become even stronger if the concentration of these alloying elements is increased further and these elements then might actually stabilize the η-phase. A similar effect may also occur for Fe and Co in higher concentrations in the η-phase. For the other elements where a magnetic state was found, the effect is small and probably does not affect the energies significantly.

4 Discussion

As explained in the introduction, the δ and η-phase are important in designing wrought alloys. For some alloys (like alloy 718), stabilizing the δ-phase at higher temperatures without simultaneously promoting the η-phase is an important goal, whereas other alloys like alloy 706 exploit the η-phase. It is therefore important to understand which elements may be used to selectively stabilize one of these phases.

Fig. 9 shows a plot of the calculated energies from Fig. 6 and 8. The two shaded regions show which elements can be used to stabilize one phase more strongly than the other, with elements close to the boundary between the regions stabilizing both phases.

Elements that strongly favor the δ-phase are Mo, Tc, Re, Os, and W. The elements V, Ta, Ru, Ag, and Au also stabilize the δ-phase more strongly than the η-phase, but the effect is of the order of the thermal energy at forging temperature ($k_B T \approx 100$ meV). The η-phase is strongly stabilized by Al and Zn. For Cd, Rh, and Hg, the energy in the η-phase is close to that in the δ-phase so that both phases may be stabilized. This is also true for Zr and Hf which have a strong tendency to replace Nb and Ti, respectively. (At sufficiently high concentrations, Ni_3Zr or Ni_3Hf may form instead.) Note that among these elements, Hg, Cd, Ag, Au are known to strongly deteriorate mechanical properties of the alloys and are thus not suitable as alloying elements.

Although the δ and η-phase are non-magnetic, alloying elements may change the magnetic state of these phases. This effect is largest for Cr, Mn, Fe, and Co. For the δ-phase, these elements have large energies in the δ-phase and do not dissolve in this phase according to our calculations, but for the η-phase, magnetic effects may actually allow these elements to dissolve. It can also be expected that increasing the concentration of these elements will increase this effect further.

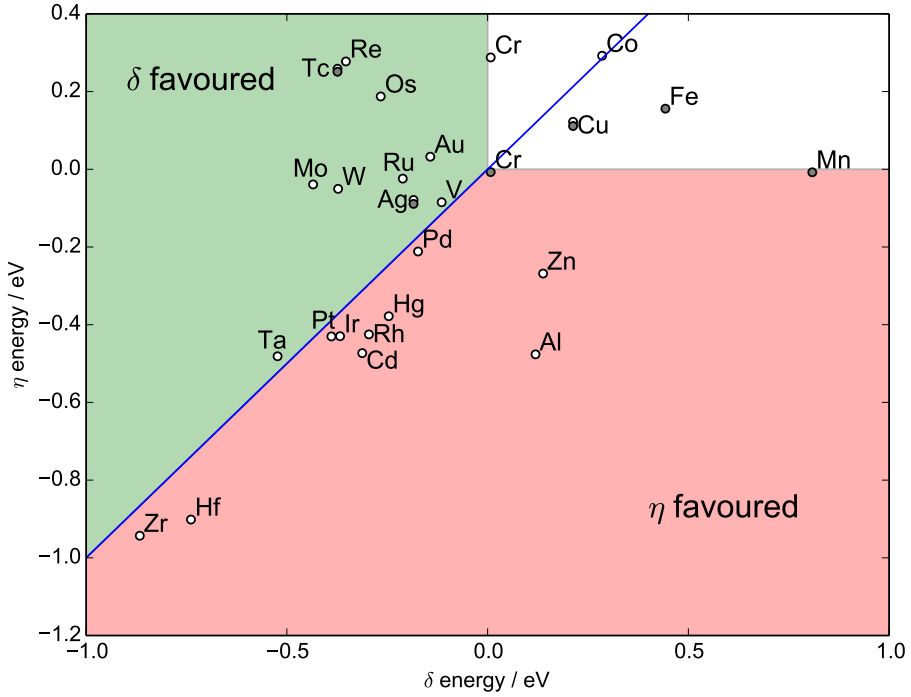

Figure 9: Effect of alloying elements on the stability of the δ-phase and η-phase. The plot shows the energy change in adding an element to both phases. Elements in the upper left region tend to stabilize the δ-phase more strongly than the η-phase; those in the lower right region stabilize the η-phase more strongly. Datapoints in grey are for configurations with magnetic moment in the δ or η-phase; datapoints for the non-magnetic state of Fe and Mn in the η-phase are not shown because they are outside of the scale (larger than 1 eV).

In the calculations presented here, a $Ni_{31}X$-supercell was used to represent the γ-phase. In realistic nickelbase superalloys, the γ-phase contains a large number of alloying elements. One of these elements is chromium which has the effect of making the alloy non-ferromagnetic. A full study of a 32-atom supercell with the appropriate amount of Cr-atoms (typical Cr contents are about 18%) would require the computation of a large number of different configurations and is beyond the scope of this paper. To estimate the size of the effect, we performed some preliminary calculations using a smaller $Ni_{14}Cr_2$ cell. We chose the lowest-energy state we found for this cell as a reference and then substituted one Ni atom by the alloying element in different positions. The solution energies of most elements tend to decrease on the order of about 200 meV, so that dissolving elements in the chromium-containing matrix becomes more favourable. Thus it may be expected that the phase-strengthening effect of some elements may be weakened by this effect. A more detailed study of this effect will be done in the future.

In conclusion, our results give theoretical insights into the stabilizing effects of relevant alloying elements on the δ and η-phase. All calculations were performed at 0 K. Additional studies are thus necessary to see how finite-temperature effects affect our results. In addition, EDX-measurements of the δ and η-phase will be performed to compare these results to experiments.

Acknowledgements

The DFT simulations were performed with resources provided by the North-German Supercomputing Alliance (HLRN).

References

[1] WD Kennedy and RL Cao. New development in wrought in 718-type. *Acta Metall*, 18(1):39–46, 2005.

[2] Xi Shan Xie, Jian Xin Dong, and Mai Cang Zhang. Research and development of Inconel 718 type superalloy. In *Materials science forum*, volume 539, pages 262–269. Trans Tech Publ, 2007.

[3] Robert E Schafrik, Douglas D Ward, and Jon R Groh. Application of alloy 718 in GE aircraft engines: past, present and next five years. *Superalloys*, 718:625–706, 2001.

[4] Peter W Schilke, JJ Pepe, and Robin C Schwant. Alloy 706 metallurgy and turbine wheel application. *Superalloys*, 718(625,706):1, 1994.

[5] RL Kennedy. ALLVAC® 718PLUS™, superalloy for the next forty years. *Superalloys*, 718:625–706, 2005.

[6] T Fedorova, J Rösler, B Gehrmann, and J Klöwer. Invention of a New 718-Type Ni-Co Superalloy Family for High Temperature Applications at 750 C. In *8th International Symposium on Superalloy 718 and Derivatives*, pages 587–599. Wiley Online Library, 2014.

[7] Xiaoxia Wu and Chongyu Wang. Density functional theory study of the thermodynamic and elastic properties of Ni-based superalloys. *Journal of Physics: Condensed Matter*, 27(29):295401, 2015.

[8] G Kresse and J Hafner. Ab initio molecular-dynamics simulation of the liquid-metal–amorphous-semiconductor transition in germanium. *Physical Review B*, 49(20):14251, 1994.

[9] Georg Kresse and Jürgen Furthmüller. Efficient iterative schemes for ab initio total-energy calculations using a plane-wave basis set. *Physical Review B*, 54(16):11169, 1996.

[10] Georg Kresse and Jürgen Furthmüller. Efficiency of ab-initio total energy calculations for metals and semiconductors using a plane-wave basis set. *Computational Materials Science*, 6(1):15–50, 1996.

[11] Peter E Blöchl. Projector augmented-wave method. *Physical Review B*, 50(24):17953, 1994.

[12] Georg Kresse and D Joubert. From ultrasoft pseudopotentials to the projector augmented-wave method. *Physical Review B*, 59(3):1758, 1999.

[13] John P Perdew, Kieron Burke, and Matthias Ernzerhof. Generalized gradient approximation made simple. *Physical review letters*, 77(18):3865, 1996.

[14] G Kresse and O Lebacq. Vasp manual, 2013.

[15] Francis Birch. Finite elastic strain of cubic crystals. *Physical Review*, 71(11):809, 1947.

[16] James E Saal, Scott Kirklin, Muratahan Aykol, Bryce Meredig, and Christopher Wolverton. Materials design and discovery with high-throughput density functional theory: the open quantum materials database (OQMD). *Jom*, 65(11):1501–1509, 2013.

[17] Stefano Curtarolo, Wahyu Setyawan, Shidong Wang, Junkai Xue, Kesong Yang, Richard H Taylor, Lance J Nelson, Gus LW Hart, Stefano Sanvito, Marco Buongiorno-Nardelli, et al. AFLOWLIB. ORG: A distributed materials properties repository from high-throughput ab initio calculations. *Computational Materials Science*, 58:227–235, 2012.

[18] R Grau-Crespo, S Hamad, CRA Catlow, and NH De Leeuw. Symmetry-adapted configurational modelling of fractional site occupancy in solids. *Journal of Physics: Condensed Matter*, 19(25):256201, 2007.

[19] AK Jena and MC Chaturvedi. The role of alloying elements in the design of nickel-base superalloys. *Journal of Materials Science*, 19(10):3121–3139, 1984.

[20] C Slama and M Abdellaoui. Structural characterization of the aged Inconel 718. *Journal of alloys and compounds*, 306(1):277–284, 2000.

[21] Zahra Tarzimoghadam, Michael Rohwerder, Sergiy Vasil Merzlikin, Asif Bashir, L Yedra, S Eswara, Dirk Ponge, and Dierk Raabe. Multi-scale and spatially resolved hydrogen mapping in a Ni–Nb model alloy reveals the role of the δ phase in hydrogen embrittlement of alloy 718. *Acta Materialia*, 109:69–81, 2016.

[22] H Sugimura, Y Kaneno, and T Takasugi. Alloying Behavior of Ni3M-Type Compounds with D0a Structure. *Materials transactions*, 52(4):663–671, 2011.

[23] Yoon-Uk Heo, Masaki Takeguchi, Kazuo Furuya, and Hu-Chul Lee. Transformation of DO 24 η-Ni 3 Ti phase to face-centered cubic austenite during isothermal aging of an Fe–Ni–Ti alloy. *Acta Materialia*, 57(4):1176–1187, 2009.